

# Energy production and conversion applications of one-dimensional semiconductor nanostructures

Surojit Chattopadhyay<sup>1\*</sup>, Li-Chyong Chen<sup>2</sup> and Kuei-Hsien Chen<sup>2,3\*</sup>

National Yang Ming University, National Taiwan University and Academia Sinica, Taiwan

**One-dimensional semiconductor nanomaterials form the basis for new technologies as well as driving the evolution of existing ones. Although these various technologies are in different stages of development, from nucleation to pilot production, it is difficult to ignore the tremendous potential they carry, overall, for next-generation concepts. One of the several areas that have been revolutionized by one-dimensional nanostructures, and which could not have happened at a more critical time, is energy. This review outlines the impact that one-dimensional semiconductor materials are having on energy production and conversion technologies. Instead of being extensive, we provide key developments in the areas of light-emitting diodes, solar cells, photoelectrochemistry and fuel cells.**

With the projected world demand for energy reaching 612 quadrillion Btu ( $\sim 649 \times 10^{18}$  J or 33 GW-yrs) in 2020 and the associated problem of carbon emission, it has become necessary to look for every enabling technology that may assist in reaching that goal in a sustainable way. This daunting task can broadly be classified into two areas of research. The first area includes enhancing the efficiencies of existing ‘power-consuming’ technologies as well as energy generation and conversion. For example, the use of light-emitting diodes (LEDs) may push external efficiencies up to 50%, against 13% for conventional technologies such as fluorescent lamps. The use of sustainable energy generation by solar photovoltaics not only contributes to energy supply but also controls carbon emission. The second area includes efficient energy-storage systems, such as fuel cells and lithium batteries, for the portable electronic devices that continue to percolated throughout human society.

The advent of nanoscience has shed light on almost every field of science and technology, particularly in the development of renewable energies. Among the vast varieties of nanomaterials that have been developed, one-dimensional (1D) nanomaterials with their inherent large specific surface areas and continuous transport path for charge carriers are useful for energy harvesting and conversion applications, which are mostly associated with surface reaction and carrier transport. When the diameter of a material is reduced below a critical value, the additional advantage of 1D materials, such as surface band bending-enhanced photoconductivity or even ballistic transport, may appear, which further enhances their carrier transport properties and hence energy conversion efficiency. Extensive investigations have been made in this direction aiming to enhance the efficiency of energy conversion and harvesting while lowering the cost of the aforementioned devices. In this review, selected 1D nanomaterials and their applications in energy conversion and generation technologies such as photonics, photovoltaics, photocatalysis and fuel cells will be covered.

## Solid-state lighting and LEDs

Increased technology efficiency will eventually lower the demand for energy. For example, approximately 20% of world energy demand is

for lighting purposes, which can be reduced through the efficient use of LEDs instead of the fluorescent, incandescent or high-pressure discharge lamps commonly used today. Group III nitride materials such as AlN, GaN and InN dominate in the field of LEDs. However, ternary and quaternary compounds arising out of a mix of these, for example  $\text{Al}_x\text{Ga}_{1-x}\text{N}$  and  $\text{In}_x\text{Ga}_{1-x}\text{N}$ , can have their bandgaps, and hence emission, tuned from deep ultraviolet (UV) to the infrared by adjusting the composition fraction  $x$  [1]. These materials are hard to grow due to the scarcity of lattice-matched substrates, which has led to defects in the crystal that deteriorate the device's optoelectronic properties. One-dimensional nanowires (NWs), on the other hand, have small cross-sections and can accommodate higher levels of strain without forming dislocations. They also rapidly exclude materials forming near the growing walls, terminating propagation through the crystal. The LED, which is a forward-biased junction of a p-type (hole-transporting) and n-type (electron-transporting) material, can be downsized by the use of 1D NWs and also benefit, in efficiency, from the superior electronic [2–4] and thermal [5] transport properties compared with their bulk counterparts. One of the challenges is doping the NWs, and the other is, of course, achieving a good electrical p–n junction. Results of doping arrived with InP NWs being doped with tellurium and zinc, giving rise to n-type and p-type conductivity, respectively [6]. These NWs can then be assembled in a crossed-wire p–n junction, involving two different NWs, exhibiting the signature rectifying behavior. Under forward bias, these crossed NW junctions yield light under low operating voltages. A more facile approach soon followed where one or several p–n homojunctions could be achieved, in the axial direction, on a single NW by modulation doping [7]. The final requirement for producing a LED using this approach was to form contacts at both ends of the NWs. The next step was taken where a radial heterostructure (core–shell, p–n type) NW (Figure 1(a)) was synthesized and after selective etching of the shell (Figure 1(b)) was electrically connected at the exposed core and top shell layer allowing carrier injection (Figure 1(c)) [8]. The core, boron-doped silicon NW (diameter,  $\sim 80$  nm), was fabricated using a conventional gold catalyzed vapor-liquid-solid (VLS) process. The shell, polycrystalline CdS (shell thickness, 60 nm), was deposited by pulsed laser deposition [8].

\*Corresponding author. Email: sur@ym.edu.tw (S.C.), chenkh@pub.iams.sinica.edu.tw (K.-H.C.)

<sup>1</sup>Institute of Biophotonics, National Yang Ming University, Taipei 112, Taiwan

<sup>2</sup>Center for Condensed Matter Sciences, National Taiwan University, Taipei 106, Taiwan

<sup>3</sup>Institute of Atomic and Molecular Sciences, Academia Sinica, Taipei 106, Taiwan

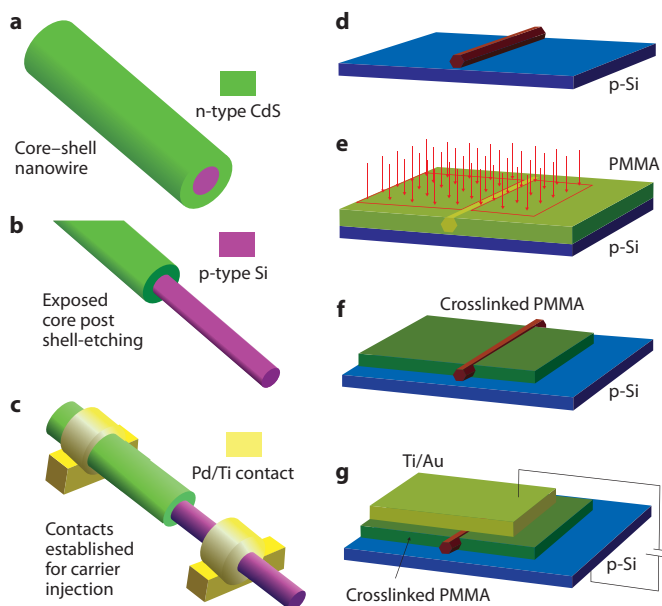


**Figure 1.** Schematics of (a–c) a single core-shell NW heterostructure LED and (d–g) the procedure for fabricating a metallic contact on the top surface of a single NW. (d) ZnO NWs are dispersed on a p-Si substrate. (e) A poly(methyl methacrylate) (PMMA) thin film (~120 nm) is spin-coated on the substrate. The wire is located and imaged by scanning electron microscopy (SEM) using a focused ion beam system. The pattern for electron beam exposure is defined directly on the SEM image (red outline) and subsequently written. The dose is ~10 mC cm<sup>-2</sup>, which is 15–20 times higher than the dose for positive exposure. (f) The unexposed and partially exposed PMMA is removed by immersing the sample in acetone for 5 min, then washed with isopropyl alcohol and dry cleaned with nitrogen air. As PMMA shrinks when cross-linked, the thickness of the film reduces to ~90 nm. (g) Ti/Au is deposited using an electron-beam evaporator to form the top metallization. Figures (d–g) modified after Ref. 9 (© 2006 ACS).

Other techniques for achieving single NW LED structures are not scarce. In one such case, a ZnO NW (n-type) and silicon wafer (p-type) junction was demonstrated using poly(methyl methacrylate) (PMMA) as a negative photoresist (Figures 1(d–g)) [9]. A similar design of combining an NW (n-GaN) with a planar material (p-GaN) to achieve the p–n homojunction has also been demonstrated for high-brightness GaN LEDs emitting in the wavelength range of 411–437 nm [10].

Instead of a single or multiple NWs lying in the plane of the wafer, an NW jungle grown vertically on the substrate can also be used as an LED. Manganese-doped GaN NWs (p-type) grown by a nickel-catalyzed VLS process on n-type SiC substrates demonstrated LED performance [11]. These NWs belong to the special dilute magnetic semiconductor (DMS) class. ZnO NWs have also been used for vertical LEDs [12]. Making ohmic contacts at both ends is no trivial exercise, as can be seen from the complexity in composition of such contacts. The limited availability of semiconductors with a range of, or tunable, bandgaps posed the next level of difficulty, since it is the bandgaps that control the color of the emitted light by an LED.

Primary color, UV and white LEDs have been obtained, but secondary colors have been difficult to produce. A white LED based on InGaN nanodisks sandwiched between p- and n-type GaN nanorods (NRs) grown on Si(111) substrates has been recently reported [13]. Plasma-assisted molecular beam epitaxy (PAMBE) has been used to grow highly crystalline GaN NRs on which strain-free InGaN nanodisks have been deposited (Figure 2(a)) for white light emission (Figure 2(b)). The GaN NRs behave as templates for the In<sub>x</sub>Ga<sub>1-x</sub>N nanodisks, which are tuned to have a range of optical emission properties by modulating the composition fraction ( $x$ ) through control of deposition temperature. Higher deposition temperatures resulted in smaller  $x$  values and hence a blue shift of emission influenced by the GaN. Different numbers and

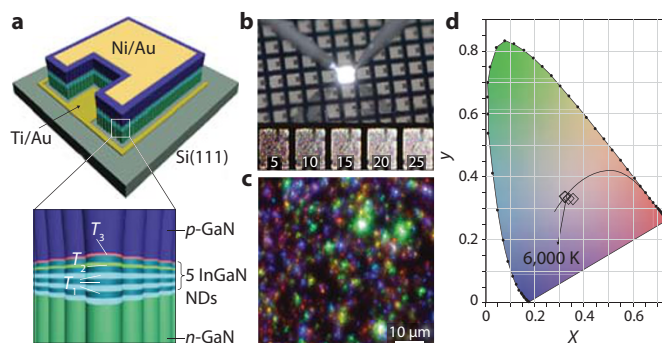


**Figure 2.** (a) Schematic of NR-array LED structure for generation of white light. The active regions contain multiple InGaN nanodisks. (b) Photograph of NR array LED emitting white light under 20 mA injection current. Micro-electroluminescence images are acquired using a 10 $\times$  objective lens at various injection currents. (c) Micro-electroluminescence image (20 mA) under 100 $\times$  magnification, revealing full-visible-spectrum emissions from the white LED. (d) Commission Internationale de L'Éclairage 1931 chromaticity coordinates at injection currents at 5–25 mA. The correlated color temperature (shown on the Planckian locus) remains near 6,000 K (natural white light) for injection currents larger than 5 mA. Modified after Ref. 13 (© 2010 AIP).

compositions of nanodisks ensured light emission over a broad visible spectral range from 450 to 700 nm (Figure 2(c)), the mixture of which produced the effective white light (Figure 2(d)) at the microscale [13].

Although 1D NWs are now integral to the field of LEDs, a great deal needs to be done in order to deliver photons using 1D NW-based LEDs to integrated optical systems and fiber-optics. Photonic devices rely heavily on the coupling efficiency of the light source, such as an LED, to a fiber-optic or a photonic waveguide, which may then be used for optical communication or processing. Although not in an LED form, optically or electrically driven single NW systems have been used to illuminate photonic crystal waveguides [14]. Here, a VLS-grown active CdS NW (diameter, 80 nm; length, 5  $\mu$ m; emission, 510 nm) is embedded in a Si<sub>3</sub>N<sub>4</sub> photonic crystal slab that is transparent at 510 nm (Figures 3(a,b)). The two-dimensional (2D) photonic crystal is specially designed so that the guided mode overlaps with the CdS emission wavelength of 510 nm. Holes were made in the Si<sub>3</sub>N<sub>4</sub> film by electron-beam lithography to construct the photonic crystal (Figure 3(b)). The structural parameters of the photonic crystal, with a lattice constant of 185 nm and hole diameter of 92.5 nm (Figure 3(b), left inset), were calculated so as to produce a bandgap of 510 nm. In this way, the straight single-line defect waveguide can transport the CdS NW emission when the latter is optically excited (Figure 3(c)). The intensity and spectral quality of the input and output beams at the excitation and collection points are shown in Figure 3(d). Even electrically driven LED systems were shown to deliver light in such photonic crystals [14]. The use of 1D nanostructure materials and techniques to incorporate them in devices have not only revolutionized the field of solid-state lighting but also shaped the future for nanophotonics and all-optical processing.

In summary, NW-based LEDs have come a long way and the technology is developing fast toward commercialization, riding the needs of the automotive, medicine and display industries. The efficiencies are quickly reaching technological break-even thresholds. GloAB, a Lund University spin-off developing NW LEDs, is beginning pilot production at DTU Danchip. Although the available colors are still limited, the advent of white LEDs is a boost to this field and we can be hopeful of some significant advances in display technologies in the near future.

## Photovoltaics

A device design based on a structure similar to that of 1D nanostructure-based LEDs but utilizing the reverse process, without any requirement for biasing, could result in a solar cell with an overall efficiency close

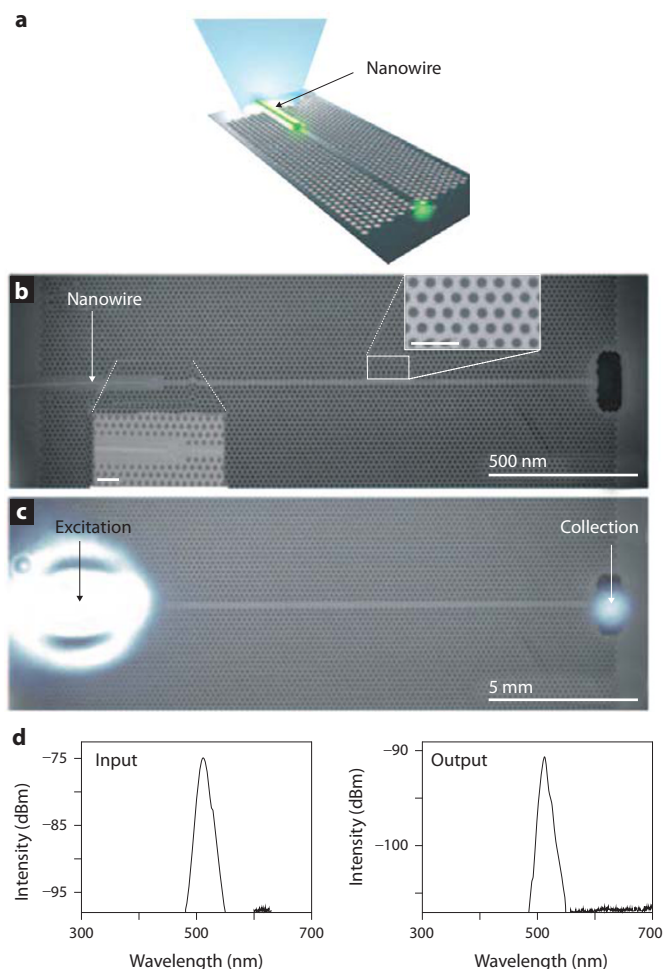


**Figure 3.** Optical injection from a semiconductor CdS NW into a photonic crystal waveguide. (a) Schematic of 2D photonic bandgap structure in an  $\text{Si}_3\text{N}_4$  slab with straight line-defect waveguide aligned with the CdS NW. (b) Scanning electron microscopy (SEM) image of CdS NW facing the straight waveguide terminated with a large hole used as an output scattering site, and magnified SEM images of the NW (inset, left) and the photonic crystal structure (inset, right). Inset scale bars, 500 nm. (c) Photoluminescence superimposed on the SEM image of (b). (d) Photoluminescence spectra of NW emission and light scattered from the photonic crystal waveguide output. The output power was measured at the spectrometer. Modified after Ref. 14 (© 2008 NPG).

to that determined by the number of electron–hole pairs collected at the electrodes per incident photon. Crystalline silicon technology currently dominates the market, with competition from non-silicon polycrystalline materials such as cadmium telluride, copper indium gallium selenide and amorphous silicon technologies, each of which have pros and cons of their own. The superior size-dependent transport properties of 1D nanostructures, however, makes them ideal for efficient carrier collection. Conventional solar cells use expensive high-purity single-crystalline materials in order to maximize the minority carrier diffusion length. One-dimensional nanostructure-based solar cells ease such a requirement through the application of three basic designs or architectures: axial heterostructures with junctions (one or several) along the length of the NW, radial heterostructures with junctions along the radial direction of the NWs, and 1D arrays (p- or n-type) embedded in an absorber (n- or p-type).

Each of these designs have their advantages and limitations. For example, the radial heterostructure and NW-embedded in an absorber architectures have significantly large junction areas and reduced minority carrier collection length. The radial and axial heterostructures have a three-dimensional (3D) geometry for reduced reflection loss and

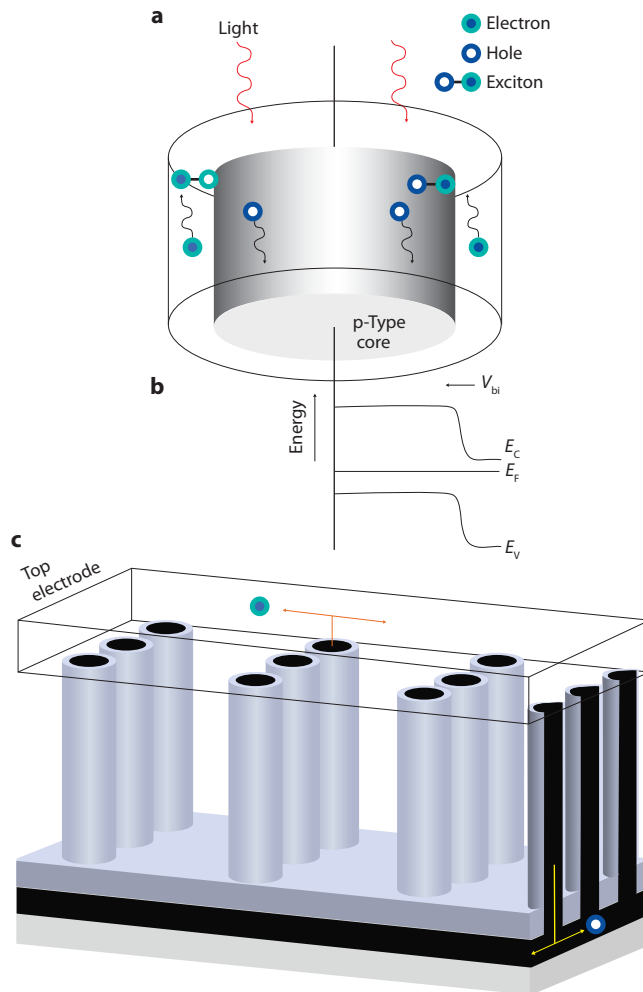


**Figure 4.** (a) Schematic of a core-shell (p-n junction) single-NW radial heterojunction showing exciton generation by the absorption of light and dissociation by the built-in field ( $V_{bi}$ ), with subsequent diffusion of the free electrons and holes to the top and bottom electrodes, respectively. (b) Energy band diagram and  $V_{bi}$  across the radius of the core (p-type) and shell (n-type) structure. (c) Schematic of solar cell device showing carrier collection.

a single-crystalline axis for superior charge transport. Increases in the surface and junction areas, at the nanoscale, also result in unwanted increases in recombination events. Hence, materials with low surface recombination velocities are desired for 1D nanostructure-based solar cells. In short, both design and material aspects are critical for achieving solar cells with efficiencies comparable to those for single-crystalline and thin-film cell designs.

Axial (p-n) heterojunctions, reported for silicon NWs, produced by modulation doping (boron and phosphorus) resulted in single-NW solar cells with low open circuit voltage ( $V_{oc}$ ) and short circuit current density ( $J_{sc}$ ) [15]. Both of these parameters were improved with the introduction of an intrinsic (i) layer at the heterojunction to achieve a p-i-n axial heterostructure solar cell. The performance of such devices increases with the length of the i segment. The best power conversion efficiency (PCE) ( $(FF \times J_{sc} \times V_{oc}) / P_{in}$ ;  $FF$ , fill factor,  $P_{in}$ , incident photon power) of 0.5% was estimated for a 4  $\mu\text{m}$  i segment using a projected area calculation [15]. Tandem cells with p-i-n<sup>+</sup>/p-i-n<sup>-</sup> ( $i = 2 \mu\text{m}$ ) structures have also been demonstrated, showing ~40% higher  $V_{oc}$  ( $= 0.36 \text{ V}$ ) compared with the single-NW axial p-i-n ( $i = 4 \mu\text{m}$ ) device [15].

In radial heterojunctions with p-n junctions along the radial direction of the wire, photons are absorbed (Figure 4(a)) in a direction perpendicular to charge separation, that is, the direction of the built-in

potential ( $V_{bi}$ ) of the p–n junction (Figure 4(b)). This is the key in 1D nanostructure-based solar cells, as depicted in Figure 4(a), where a radial homo- or heterojunction NW array composed of a p-type core and n-type shell is shown [16]. The substrate (bottom electrode) is electrically connected to the cores, whereas the top electrode is connected to the shells of the NWs (Figure 4(c)).

The diameters of the wires have to be designed to be less than twice the minority carrier diffusion length (100–1,000 nm) [17,18]. This type of nanoscale design will be particularly helpful when the carrier diffusion lengths are small, that is, the material is highly defective. Single-junction (p–n) cells with PCEs of 0.5% [19] have been shown, but these devices suffer from high dark current and high resistivity of the polycrystalline shell layer [20], reducing  $J_{sc}$ . An improvement in shell resistivity could improve  $J_{sc}$  by a factor of four, with similar  $V_{oc}$ , and also enhance PCE to values of 2.3–3.4% for a single-Si-NW photovoltaic device (structure similar to that shown in Figure 1(c)) [21]. Single-Si-NW photovoltaic devices with p–i–n radial heterostructures demonstrated nearly five times higher  $J_{sc}$  and 15 times higher maximum power output (72 pW) at 1 sun compared with a similar p–i–n axial heterostructure [21]. As a natural extension to the p–n radial heterostructure design, tandem radial heterostructures (p–n/p–n/p–n) of InGaN/GaN multiple quantum well features have been developed using bottom-up growth techniques with precise control of deposition parameters [22].

Instead of conventional inorganic semiconductors, in some cases small molecules, quantum dots (QDs) or polymers could also be used as the absorber material. Unlike conventional solar cells, in which the photogenerated excitons (electron–hole pairs) can be easily dissociated by room-temperature thermal energy ( $kT \approx 26$  meV;  $T$ , temperature,  $k$ , Boltzmann constant), excitons in organic dyes or polymers have much higher binding energies. For charge separation, these excitons have to diffuse to the p–n junction where a sufficient band-offset or  $V_{bi}$  is available to dissociate the exciton (with efficiency  $\eta_{ED}$ ) and send the free charge to the respective electrodes for collection (with efficiency  $\eta_{CC}$ ) (Figure 5(a)). Hence, there are two limiting factors for charge separation in such a structure: the small exciton diffusion length ( $\sim 10$  nm in polymers, up to a 1  $\mu\text{m}$  in small molecules) [23], and charge injection across the junction. The solution to these limiting factors lies in designing large-area junctions oriented normal to the substrate, increasing the absorber volume, and enhancing the efficiency of the charge transport pathways [24]. The possible use of 1D nanostructures is evident (Figures 5(b,c)).

Although polymer materials such as poly(3-hexylthiophene) (P3HT) or [6,6]-phenyl- $C_{61}$ -butyric acid methyl ester (PCBM) have short exciton diffusion lengths and extremely low hole mobilities ( $10^{-1}$  to  $10^{-7}$   $\text{cm}^2 \text{V}^{-1} \text{s}^{-1}$ ), their optical absorption coefficient is high ( $\sim 10^5$   $\text{cm}^{-1}$ ). Hence, a polymer-based solar cell may not require a large thickness of medium for optical absorption (with efficiency  $\eta_A$ ), and use in combination with an inorganic component [24,25] could compensate for the short diffusion length and low hole mobility. Hybrid devices consist of an interpenetrating network of electron-accepting and -donating materials to form bulk heterojunctions (Figure 5(b)). The p–n junctions are not limited to a single plane and are distributed throughout the bulk of the absorbing material (Figures 5(b,c)). Such bulk-heterojunction devices may use all-organic blends, fullerene derivative–polymer blends or NW–polymer blends. The external quantum efficiency ( $\eta_{EQE}$ ) of such excitonic cells is given by  $\eta_{EQE} = \eta_A \eta_{ED} \eta_{CC}$  (Figure 5(a)). The all-organic cells can achieve efficiencies up to 5% with  $\eta_{ED} \approx 1$  [26]. In contrast to solar cells based on composites of nanoparticle (NPs) and a polymer, which can produce efficiencies of  $\eta_{EQE} \approx 2.6\%$  [27], excitonic solar cells incorporating ZnO NWs or NRs solar cells can have efficiencies of up to  $\eta_{EQE} \approx 14\%$  but with PCEs of 0.2% [28]. The incorporation of ZnO into P3HT quenches photoluminescence, indicating a higher  $\eta_{ED}$ . However, the addition of a thin ( $\sim 5$  nm) polycrystalline  $\text{TiO}_2$  shell on the ZnO NRs can improve the efficiency by a factor of five compared with the pure ZnO NRs [29]. Similar improvements were obtained with an MgO shell on a ZnO core [30], however in both cases, the efficiencies were limited to 0.4%. Using longer ZnO NWs in a P3HT:PCBM

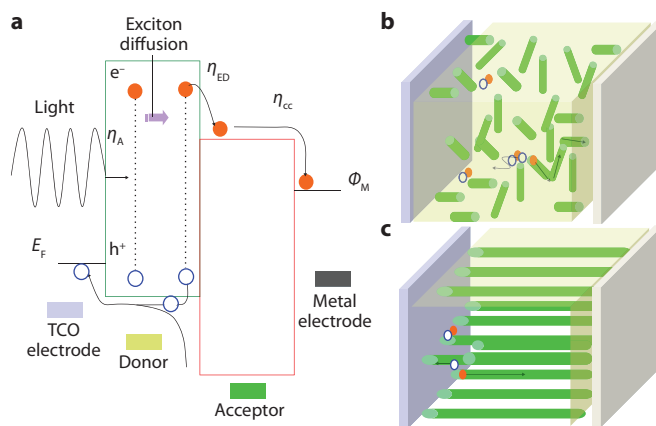


**Figure 5.** (a) Schematic of the band arrangement in bulk heterojunction solar cells. Light absorbed at the donor creates excitons, which diffuse to the junction where they are dissociated. The electrons ( $e^-$ ) migrate to the metal electrode, with work function  $\Phi_M$ , and the holes ( $h^+$ ) migrate toward the transparent conducting oxide (TCO) electrode. (b,c) Schematics of donor–acceptor heterojunction solar cells with (b) polymer-NW and (c) polymer-NW array structures. The exciton dissociation and electron and hole transport paths are indicated by arrows. Color assignments match those in (a).

device produced efficiencies of  $\sim 4\%$ . Evidently, the ZnO NWs are better charge conductors than PCBM, and also contribute positively to  $J_{sc}$  [31]. Hybrid structures of InP NWs and P3HT have also been tried as photodiodes with good  $FF$  ( $\sim 0.44$ ) but low  $J_{sc}$  [32]. Here, the n-InP NWs were grown on indium tin oxide electrodes and enveloped with p-type P3HT.

The most efficient and stable of the excitonic solar cells are the dye-sensitized solar cells (DSSCs), in which a dye (ruthenium polypyridine) is used for optical absorption dispersed on a nanostructured inorganic material such as  $\text{TiO}_2$  NPs as an electron transport material [33]. The  $\text{TiO}_2$  is grown on a fluorine-doped tin oxide electrode with platinum for the cathode, and the whole assembly immersed in a triiodide/iodide ( $\text{I}_3^-/\text{I}^-$ ) redox couple (electrolyte) and sealed. Excitons created at the dye are dissociated at the dye–inorganic interface with the electrons being transported by the inorganic phase as the electrolyte is oxidized. The electrons, after completing the load circuit, are delivered back to the electrolyte (reduction) via the platinum electrode. Although the PCEs for this architecture are high ( $\sim 11\%$  [33]), the method has drawbacks in the use of an corrosive electrolyte and expensive cathode (platinum) material. These problems have been addressed recently by Graetzel’s group, who invented the DSSC in 1991. By using cobalt sulfide as the cathode material [34], replacing platinum and using a new disulfide/thiolate ( $\text{T}_2/\text{T}^-$ ) redox couple [35] in which  $\text{T}^-$  is 5-mercapto-1-methyltetrazole ion and  $\text{T}_2$  is its dimer, Graetzel’s group was able to produce a stable DSSC with PCE of up to 6.4%. The new electrolyte is not only less corrosive but also has no absorption in the visible region, unlike the triiodide/iodide electrolyte.

The use of low-resistivity ( $< 2.0 \Omega \text{ cm}$ ) and high field effect mobility ( $\sim 5 \text{ cm}^2 \text{V}^{-1} \text{s}^{-1}$ ) NWs such as vertically arrayed ZnO instead of an interrupted network of NPs creates better transport pathways for electrons. Unlike the mesoporous  $\text{TiO}_2$  NP film, the NWs are thick enough to support a depletion zone near the surface, which provides a field for efficient exciton dissociation. In addition, the energy band inside the NWs is bent at the surface, providing a slope for the electrons to be swept toward the center of the NWs, reducing the chances of recombination. The effect of band bending is considerable for small-diameter NWs. In the absence of counter-ions in the electrolyte, the electrons in the NW are subject to an internal electric field along the axial direction, which drives the electrons to the collection electrode. Despite these theoretical advantages, however, ZnO NW-DSSCs have been unable to exceed a PCE of 1.5% ( $\eta_{EQE} \approx 45\%$ ,  $FF = 0.45$ ,  $V_{oc} = 0.68$  V,  $J_{sc} = 6$   $\text{mA cm}^{-2}$ , AM 1.5 illumination) [36]. The unexpectedly poor performance of this

design is attributed to the lower surface area for dye dispersion compared with the NPs, and hence lower optical absorption, which limits exciton generation. Under the same dye-loading conditions (same amount of dye per unit thickness of cell), the NW-DSSCs do have better  $J_{sc}$  compared with the corresponding NP-DSSCs. However, the  $\text{TiO}_2$  NPs produce the highest  $J_{sc}$  and efficiency, followed by vertical  $\text{TiO}_2$  NW array DSSC [37] with PCEs in the vicinity of 5%.

To increase the area for dye absorption and charge transport (and hence lower series resistance), mixtures of NPs and NWs have been tried in both the  $\text{TiO}_2$  and ZnO systems. For the  $\text{TiO}_2$  system, a 20% (by weight) NW content increased the PCE to 8.6% from 6.7% for the pure NP-DSSC [38]. For the ZnO system, the mixed NP-NW mercurochrome-sensitized DSSC saw an improvement of PCE from 0.45% (pure NP) to 2.77% ( $V_{oc} = 0.58$  V,  $J_{sc} = 8.33$  mA cm<sup>-2</sup>,  $FF = 0.58$ ) using 5.5  $\mu\text{m}$ -long NWs [39]. A longer NW array (6.2  $\mu\text{m}$ ) produced a higher PCE of 3.2% with lower  $V_{oc}$ . Hierarchical (branched tree-like) ZnO NW structures may prove to be superior to NW-DSSC systems.

The relatively poor performance of the ZnO-based DSSCs compared with  $\text{TiO}_2$  is due to surface chemical reactions [40], the aggregation of dyes [41], surface trap states [42] and slow charge injection from the dyes [43]. Remedial core-shell NWs (with a ZnO core and  $\text{TiO}_2$  shell) [44] have been used in order to benefit from the charge transport of the crystalline ZnO NW and surface stability and charge transfer characteristics of the  $\text{TiO}_2$  shell, but the approach has so far met with limited success (PCE  $\approx$  2.1%) [45]. Tin oxide NWs with an atomic layer  $\text{TiO}_2$  NPs have been used with greater success, achieving PCE of  $\sim$ 4.1% ( $V_{oc} = 0.72$  V) compared with 2.1% for the pure  $\text{SnO}_2$ -NW DSSC [46]. Solar cells employing QD-sensitized ZnO NW solar cells with a similar  $\text{I}_2/\text{I}_3^-$  redox couple (as in a DSSC) with PCE of 0.4% ( $V_{oc} = 0.6$  V) have been reported [47]. The QDDSSC system, however, has considerable scope for improvement as the QD material and size can be varied to tune the absorption range of the cell.

In a more elaborate approach, Wu *et al.* [48] used both NWs and branched hierarchical ZnO ‘nanotrees’, achieving a more than two-fold increase in PCE compared with devices based on NR structures. The N719 dye used in this approach is designed for the  $\text{TiO}_2$  DSSC system and not optimized for the ZnO system. A new dye rationally designed for better adhesion and electron transport to ZnO is therefore likely to enhance the efficiency of this new photovoltaic system.

In summary, 1D NW-based photovoltaic devices still lag, in performance, their NP-based counterparts, although the former offers better electron transport. The surface area and optical absorption issue as well as the surface recombination issues have to be better understood and controlled in order to realize performance improvements. Although the use of dyes or QDs to enhance absorption has been investigated, there is still a long way to go for any NW-based technology to become commercially viable. Material availability and architecture design for the NW-based devices is crucial, and pivotal breakthroughs in the bottom-up growth of axial and radial heterojunctions have been obtained. Although single-NW photovoltaic devices are not yet the answers to the global energy crisis, a possible scale-up of these techniques cannot be ruled out. The intense research activity in this field keeps us hopeful for some major innovations that could replace or at least challenge the conventional silicon-based technologies.

### Photoelectrochemistry

The inherent bending of electronic bands at surfaces can result in a built-in potential well in a semiconductor NW with diameter below a critical value [49,50]. Upon photoexcitation, the potential well thus established leads to a spontaneous separation of excitons into electrons and holes that propagate to the center and surface of the nanowires, respectively. This significantly reduces the recombination of carriers, promoting subsequent charge collection for efficient energy harvesting. Photoconductivity measurements have shown a responsivity

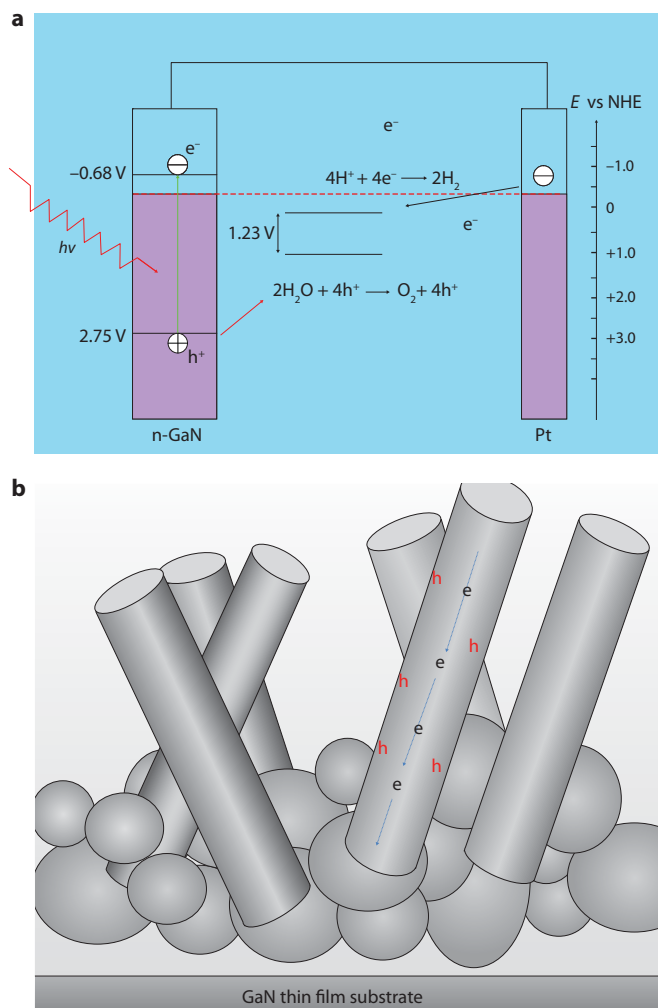


**Figure 6.** (a) Schematic of the photoelectrochemical system for water splitting using n-type GaN, showing the potential for hydrogen and oxygen evolution. A platinum counter electrode is used for hydrogen evolution. (b) Schematic of the interface between the NWs and the electrode.

enhancement of up to 1,000 times in GaN NWs compared with their thin film counterparts. Further studies have concluded that the enhancement is associated with the prolonged lifetime of carriers rather than their mobility, which is attributed to charge separation in the nanowire.

To take advantage of the spontaneous charge separation process, separate connections to the core and shell of each individual NW are needed, which is considerably difficult even with the recent advancements in nanotechnology. This difficulty can be overcome by immersing the system in an electrolyte, wherein the shells of the NWs are connected to the electrolyte while the cores are attached to the substrate. A photoelectrochemical system as depicted in Figure 6(a) illustrates this idea, which has been widely pursued in water splitting for the generation of hydrogen. Many series of experiments have been carried out to compare the efficiency of thin film and nanostructured systems for water splitting. Solar-to-hydrogen conversion efficiencies of 0.37% and 0.75% have been reported for thin film and chemically etched GaN [51]. While further enhancement of the NW system is underway, it is clear that the conductivity at the wire-to-substrate interface is critical for water splitting. As shown in Figure 6(b), for most of the chemical vapor deposition-based growth processes, substantial grain boundaries can be formed at the interface, which will severely undermine the transport of carriers created in the photoexcitation process. New techniques for the epitaxial growth of NWs on GaN substrates are needed in order to avoid the formation of multiple grain boundaries.

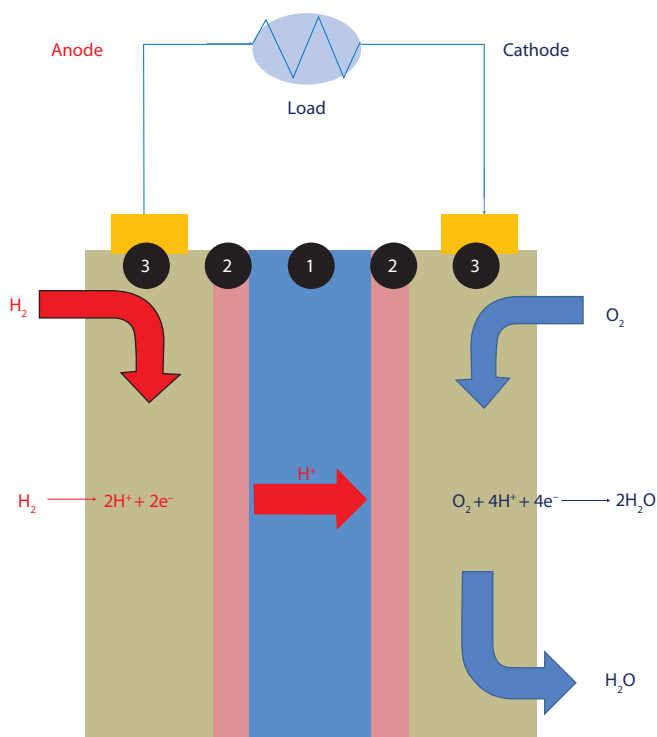
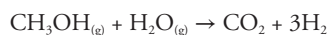


**Figure 7.** Schematic of a membrane electrode assembly in a PEM fuel cell with hydrogen and oxygen inlets in the anode and cathode, respectively, to generate electricity and water. Layer 1, proton-conducting electrolyte; layer 2, catalyst; layer 3, gas-diffusion layer.

## Fuel cells

Fuel cells are one of the cleanest energy devices and also offer the highest energy conversion efficiencies, and so are regarded as one of the best choices for future energy sources, except for their price. Hydrogen is used in fuel cells as a clean, sustainable and transportable alternative fuel for electric power generation [52]. The catalytic reformation of hydrocarbon is currently the predominant process for hydrogen generation in fuel cells, following the reaction:



Evidently, the leading technique for hydrogen generation is the catalytic reformation of methanol [53]. Cu/ZnO-based catalysts are, therefore, of great importance for the industrial-scale catalytic production of reformed hydrogen [54]. Several techniques have been reported for the production of suitable catalysts, including a commercial Cu-ZnO-Al<sub>2</sub>O<sub>3</sub> product manufactured by Süd Chemie under the name MDC-3. A recent report presented the design for a core-shell nanostructured catalyst consisting of a ZnO NR core and an outer shell of copper NPs for high-efficiency catalytic conversion [55]. This novel core-shell catalyst has a conversion efficiency of 93% and hydrogen production rate of 183 mmol g<sub>cat</sub><sup>-1</sup> h<sup>-1</sup> at 250 °C, surpassing the commercial MDC-3 by ~20% on both measures. In addition, the emission of toxic CO is reduced by about 80% under similar reaction conditions [55].

The proton-exchange membrane (PEM) fuel cell, a schematic for which is shown in Figure 7, catalytically converts hydrogen into pure water and electricity without other pollutants and at very low noise levels. However, the platinum catalyst used in both the anode and cathode amounts to about 50% of the device cost, which keeps rising with price of platinum. Substitutes for platinum and lower loading rates have been pursued intensively over the past decade.

Taking advantage of the high surface-to-volume ratio and excellent electric conduction properties of carbon nanotubes (CNTs),

Chen and Chen initiated the idea of introducing CNTs into the electrodes of direct methanol and PEM fuel cells. Figure 8 compares the conventional approach (Figure 8(a)) using a mixture of platinum NPs and carbon black with a new approach (Figure 8(b)) in which carbon black is replaced with CNTs. The CNTs provide a direct path for the transport of reaction-generated electrons. The carbon constituent of CNTs, in particular, is highly compatible with the carbon electrodes in the acidic or basic electrolytes of fuel cells. In the new approach, low interface resistance between the CNTs and the carbon electrode, and between the platinum catalysts and CNTs, is essential for cell performance.

To improve electric conduction in this system, a method for growing CNTs on the carbon electrode directly, such as through the production of a 'carbon cloth', has been developed [56]. By applying an iron catalyst to the carbon cloth before the growth of CNTs in a chemical vapor deposition process, highly aligned CNTs can be deposited on large scales. Figure 8(c) shows a transmission electron micrograph of platinum-bearing bamboo-shaped multi-wall CNTs grown directly on the carbon fibers of a carbon cloth. The catalyst in this system is deposited by either radiofrequency sputtering [57] or a colloidal process [58]. The bamboo-shaped CNTs are formed by the incorporation of nitrogen in the growth process, which has significant advantages for subsequent catalyst deposition by significantly enhancing dispersion of the catalyst material. As shown in Figure 8(c), well-dispersed and uniform-sized catalyst NPs can be deposited on the nitrogen-incorporated CNTs, which can be explained by the establishment of nucleation sites by the incorporated nitrogen. A first-principles simulation of nitrogen and boron incorporation in CNTs and their effect on subsequent platinum nucleation has been performed to elucidate the process [59]. Figure 8(d) shows a scanning electron micrograph of platinum-loaded CNTs produced using the colloidal ethylene glycol process.

The advantage of the new approach has been demonstrated by applying a Pt-Ru/CNT catalyst as an anode in a direct methanol fuel cell [60]. The reaction at the anode is the bottleneck in direct methanol fuel cells. A cell containing a commercial electrolyte membrane (Nafion) and an ETEK cathode was used together with the CNT anode for membrane electrode assembly measurement. As shown in Figure 8(e), improved internal resistance has been demonstrated using CNTs as the catalyst support, and an optimum power of 75 mW cm<sup>-2</sup> has been obtained [60]. Taking into account that only 0.4 mg cm<sup>-2</sup> of catalyst is applied in this structure, comparative with 3.0 mg cm<sup>-2</sup> in the commercial product, the improvement is significant. On the other hand, the cathode requires a higher platinum loading to maintain the high reaction rate because the oxygen reduction reaction is slower than the hydrogen oxidation reaction. A study using PEM FCs revealed that 0.05 mg cm<sup>-2</sup> platinum loading with a CNT-carbon cloth support (cathode) gave power output above 900 mW cm<sup>-2</sup>, outperforming a commercial product with 0.25 mg cm<sup>-2</sup> loading (Figure 8(f)) [61].

## Conclusions

In conclusion, it is worth mentioning that the growth of 1D nanostructures has matured to the extent that accurate control of geometry, composition, site of growth and doping is now possible. The throughput or yield of growth can be selected, though with lesser control, by the choice of growth techniques. Modulation doping or composition control, even for single NWs, is possible in the axial as well as the radial directions of the NW. Application of these 1D structures in LEDs has matured, more so than in solar photovoltaics, and is on the verge of commercialization with luminous efficacies approaching ~95 and ~55 lm W<sup>-1</sup> for cool white (color temperature >4,000 K) and warm white (color temperature <4,000 K) LEDs, respectively, compared with 20, ~60 and ~100 lm W<sup>-1</sup> for incandescent, compact fluorescent and linear fluorescent lamps. One-dimensional nanostructure-based solar photovoltaics, on the other hand, still lag conventional crystalline or thin film technologies in terms of power conversion efficiency. Limitations include

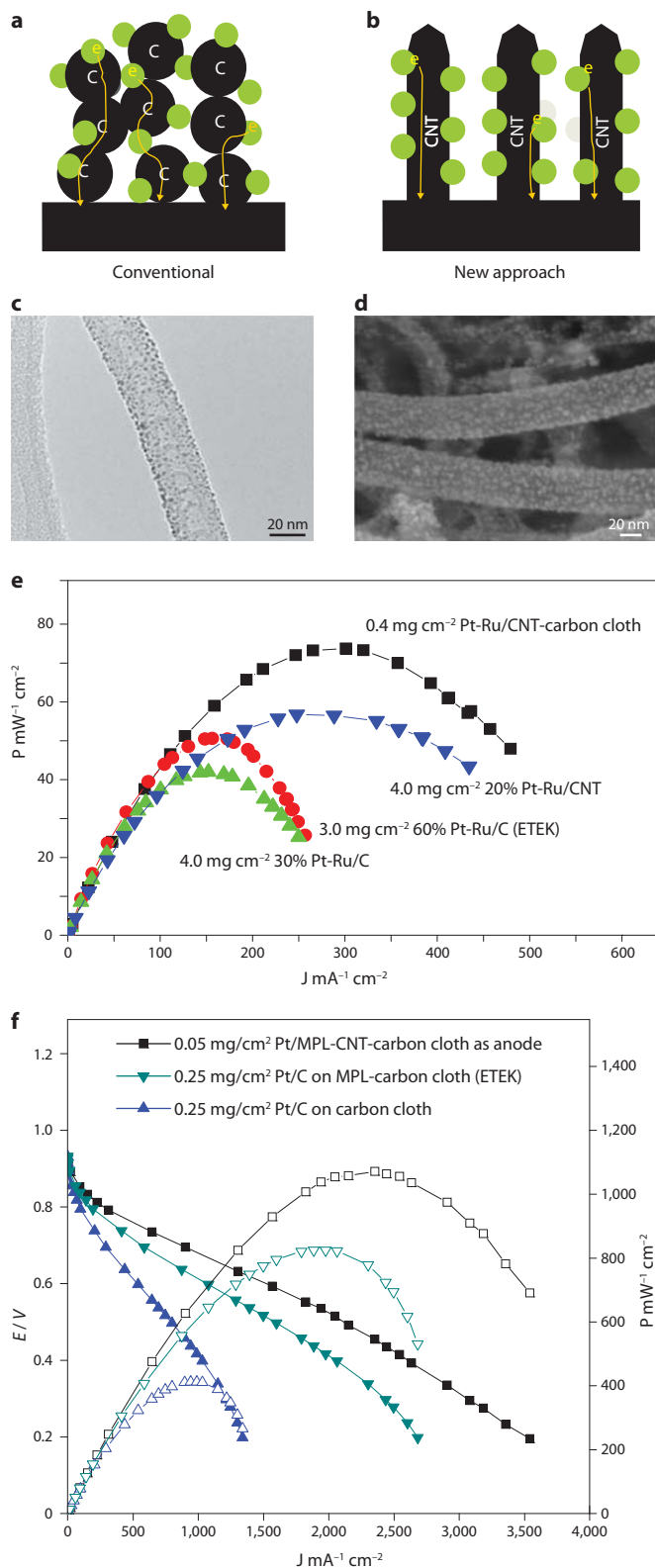


**Figure 8.** Comparison of (a) a conventional Pt/carbon black/carbon electrode structure and (b) a Pt/CNT/carbon electrode structure. (c) Transmission electron micrograph of Pt deposition on N-incorporated CNTs. Modified after Ref. 57 (© 2005 ACS). (d) Scanning electron micrograph of the same material deposited using a colloidal ethylene glycol process. (e) Polarization curves for direct methanol fuel cells utilizing CNTs as the catalyst support. Modified after Ref. 60 (© 2007 Elsevier). (f) Polarization curves for a PEM fuel cell with CNTs as catalyst support (cathode). Modified after Ref. 61 (© 2011 RSC).

both material and design/architecture aspects. Materials with strong broadband absorption, large junction area, superior charge transport channels and ease of doping are required. Some of these conditions, however, are in conflict with others, necessitating optimization. The design aspects should consider, amongst other factors, the geometry for efficient exciton diffusion and dissociation, dimension, low reflection and growth techniques. Single-NW devices are produced with axial and radial modulation, in doping (p or n) and composition (for heterostructures), for single- or multi-junction cells.

GaN NWs with diameters below 100 nm display enhanced photoelectrochemical activity for water splitting. However, the wide bandgap (3.4 eV) of GaN limits its use to UV absorption. Narrowing of the bandgap through the use of ternary In<sub>x</sub>Ga<sub>1-x</sub>N might help, although the stability of such a semiconductor in the electrolyte and under UV exposure is another challenge. Carbon nanotubes for fuel cell applications are promising. The fact that lower catalyst loading rates are needed while higher output power can be obtained is a big advantage regarding the escalating price of platinum.

Efficient nano-micro integration, such as for contacts in the devices discussed, is required for nanotechnology to transfer from the laboratory to industry. Significant steps have been and are being taken toward integrating the emerging nanotechnologies with existing energy technologies, yet many more will be needed to achieve efficient broad-based energy use for a sustainable future.

### Acknowledgements

We would like to thank the National Science Council, Academia Sinica, Taiwan, and the Air Force Office of Scientific Research and Asian Office of Aerospace Research and Development (AOARD/AFOSR) for supporting this work. The help of Lian-Jiun Li of National Taiwan Ocean University in preparing figures is gratefully acknowledged.

### References

- S. Chattopadhyay, A. Ganguly, K.-H. Chen, L.-C. Chen, *Crit. Rev. Solid State* **34**, 224 (2009).
- M. Law, J. Goldberger, P. Yang, *Ann. Rev. Mater. Res.* **34**, 83 (2004).
- W. Lu, J. Xiang, B. P. Timko, Y. Wu, C. M. Lieber, *P. Natl Acad. Sci. USA* **102**, 10046 (2005).
- Y.-J. Doh *et al.*, *Science* **309**, 272 (2005).
- D. Li, Y. Wu, R. Fan, P. Yang, A. Majumdar, *Appl. Phys. Lett.* **83**, 3186 (2003).
- X. Duan, Y. Huang, Y. Cui, J. Wang, C. M. Lieber, *Nature* **409**, 66 (2001).
- M. S. Gudixsen, L. J. Lauhon, J. Wang, D. C. Smith, C. M. Lieber, *Nature* **415**, 617 (2002).
- O. Hayden, A. B. Greytak, D. C. Bell, *Adv. Mater.* **17**, 701 (2005).
- J. Bao, M. A. Zimmler, F. Capasso, X. Wang, Z. F. Ren, *Nano Lett.* **6**, 1719 (2006).
- S.-K. Lee, T.-H. Kim, S.-Y. Lee, K.-C. Choi, P. Yang, *Phil. Mag.* **87**, 2105 (2007).
- H.-J. Choi *et al.*, *Adv. Mater.* **17**, 1351 (2005).
- R. Könenkamp, R. C. Word, C. Schlegel, *Appl. Phys. Lett.* **85**, 6004 (2004).
- H.-W. Lin, Y.-J. Lu, H.-Y. Chen, H.-M. Lee, S. Gwo, *Appl. Phys. Lett.* **97**, 073101 (2010).
- H.-G. Park *et al.*, *Nat. Photon.* **2**, 622 (2008).
- T. J. Kempa *et al.*, *Nano Lett.* **8**, 3456 (2008).
- B. M. Kayes, H. A. Atwater, N. S. Lewis, *J. Appl. Phys.* **97**, 114302 (2005).
- M. D. Kelzenberg *et al.*, *Nano Lett.* **8**, 710 (2008).
- J. E. Allen *et al.*, *Nat. Nanotechnol.* **3**, 168 (2008).
- K.-Q. Peng, Y.-J. Yan, S.-P. Gao, J. Zhu, *Adv. Mater.* **14**, 1164 (2002).
- E. C. Garnett, P. Yang, *J. Am. Chem. Soc.* **130**, 9224 (2008).
- B. Tian *et al.*, *Nature* **449**, 885 (2007).
- F. Qian *et al.*, *Nat. Mater.* **7**, 701 (2008).
- P. Peumans, A. Yakimov, S. R. Forrest, *J. Appl. Phys.* **93**, 3693 (2003).
- B. Kannan, K. Castelino, A. Majumdar, *Nano Lett.* **3**, 1729 (2003).
- K. M. Coakley, M. D. McGehee, *Chem. Mater.* **16**, 4533 (2004).
- W. Ma, C. Yang, X. Gong, K. Lee, A. J. Heeger, *Adv. Funct. Mater.* **15**, 1617 (2005).
- B. Sun, N. C. Greenham, *Phys. Chem. Chem. Phys.* **8**, 3557 (2006).
- P. Ravirajan *et al.*, *J. Phys. Chem. B* **110**, 7635 (2006).
- L. E. Greene, M. Law, B. D. Yuhas, P. Yang, *J. Phys. Chem. C* **111**, 18451 (2007).
- N. O. V. Plank *et al.*, *Nanotechnology* **19**, 465603 (2008).

31. K. Takanezawa, K. Hirota, Q.-S. Wei, K. Tajima, K. Hashimoto, *J. Phys. Chem. C* **111**, 7218 (2007).
32. C. J. Novotny, E. T. Yu, P. K. L. Yu, *Nano Lett.* **8**, 775 (2008).
33. B. O'Regan, M. Grätzel, *Nature* **353**, 737 (1991).
34. M. Wang *et al.*, *J. Am. Chem. Soc.* **131**, 15976 (2009).
35. M. Wang *et al.*, *Nat. Chem.* **2**, 385 (2010).
36. M. Law, L. E. Greene, J. C. Johnson, R. Saykally, P. Yang, *Nat. Mater.* **4**, 455 (2005).
37. X. Feng *et al.*, *Nano Lett.* **8**, 3781 (2008).
38. B. Tan, Y. Wu, *J. Phys. Chem. B* **110**, 15932 (2006).
39. C.-H. Ku, J.-J. Wu, *Nanotechnology* **18**, 505706 (2007).
40. H. Horiuchi *et al.*, *J. Phys. Chem. B* **107**, 2570 (2003).
41. T. Oekermann, T. Yoshida, H. Minoura, K. G. U. Wijayantha, L. M. Peter, *J. Phys. Chem. B* **108**, 8364 (2004).
42. Z.-M. Liao, J. Xu, J.-M. Zhang, D.-P. Yu, *Appl. Phys. Lett.* **93**, 023111 (2008).
43. J.-J. Wu, G.-R. Chen, H.-H. Yang, C.-H. Ku, J.-Y. Lai, *Appl. Phys. Lett.* **90**, 213109 (2007).
44. M. Law *et al.*, *J. Phys. Chem. B* **110**, 22652 (2006).
45. E. Palomares, J. N. Clifford, S. A. Haque, T. Lutz, J. R. Durrant, *J. Am. Chem. Soc.* **125**, 475 (2003).
46. S. Gubbala, V. Chakrapani, V. Kumar, M. K. Sunkara, *Adv. Funct. Mater.* **18**, 2411 (2008).
47. K. S. Leschkies *et al.*, *Nano Lett.* **7**, 1793 (2007).
48. S. Anandan, G.-J. Lee, P.-K. Chen, C. Fan, J. J. Wu, *Ind. Eng. Chem. Res.* **49**, 9729–9737 (2010).
49. R.-S. Chen *et al.*, *Appl. Phys. Lett.* **91**, 223106 (2007).
50. R. S. Chen *et al.*, *Small* **4**, 925 (2008).
51. A. M. Basilio *et al.*, *J. Mater. Chem.* **20**, 8118 (2010).
52. M. Z. Jacobson, W. G. Colella, D. M. Golden, *Science* **308**, 1901 (2005).
53. B. L. Kniep *et al.*, *Angew. Chem. Int. Ed.* **43**, 112 (2004).
54. Y. Choi, H. G. Stenger, *J. Power Sour.* **142**, 81 (2005).
55. Y.-G. Lin *et al.*, *Angew. Chem. Int. Ed.* **48**, 7586 (2009).
56. L. C. Chen *et al.*, *Adv. Funct. Mater.* **12**, 687 (2002).
57. C.-L. Sun *et al.*, *Chem. Mater.* **17**, 3749 (2005).
58. C. Bock, C. Paquet, M. Couillard, G. A. Botton, B. R. MacDougall, *J. Am. Chem. Soc.* **126**, 8028 (2004).
59. C.-L. Sun, H.-W. Wang, M. Hayashi, L.-C. Chen, K.-H. Chen, *J. Am. Chem. Soc.* **128**, 8368 (2006).
60. C.-H. Wang *et al.*, *J. Power Sources* **171**, 55 (2007).
61. H.-Y. Du *et al.*, *J. Mater. Chem.* **21**, 2512 (2011).

## Author profiles



### Surojit Chattopadhyay

Surojit Chattopadhyay obtained his PhD in 1996 from Calcutta University in India working at the Indian Association for the Cultivation of Science. He held the Chevening Scholarship for post-doctoral studies on amorphous silicon solar cells at the University of Dundee in UK. He worked as a postdoctoral scholar at National Taiwan University and Academia Sinica in Taiwan before joining National Chung Hsing University in Taichung, Taiwan, as an associate professor. He is currently with the Institute of Biophotonics at National Yang Ming University in Taipei, Taiwan. His research interests include functional nanomaterials, biosensors, solar cells, semiconductor optoelectronics, surface-enhanced Raman spectroscopy, biomimetics and related topics.



### Kuei-Hsien Chen

Kuei-Hsien Chen obtained his PhD in applied science from Harvard University in 1989. He worked on chemical vapor deposition of diamond at the research and development center of General Electric Corporation until 1992 before joining Academia Sinica in Taiwan. He now works in the Institute of Atomic and Molecular Sciences at Academia Sinica on the synthesis and application of optoelectronic materials, particularly in one-dimensional nanomaterials such as carbon nanotubes, graphene, GaN nanowires, and their composites. His research interests cover fuel cells, electrocatalysis, gas reforming and solar cells.



### Li-Chyong Chen

Li-Chyong Chen is currently a Distinguished Research Fellow in the Center for Condensed Matter Sciences at National Taiwan University (NTU). She earned her PhD in applied physics at Harvard University (1989) and was proffered an honorary doctoral degree from Linköping University in Sweden (2007). Prior to her appointment at NTU, she had worked at General Electric Corporate Research and Development in New York, USA (1989–1994). Over the last decade, her group has established a strong program on one-dimensional nanomaterials and related hybrids, in particular, those formed by various vapor-phase deposition techniques. The group is also specialized in integrated microdevices for optical, electrical, energy and sensing applications. She was named a Laureate of the 22nd Khwarizmi International Award, Iran, in 2009, and was honored as a Fellow of the Materials Research Society, USA, in 2010.